

Energy Level Engineering in Transition-Metal Doped Spinel-Structured Nanosheets for Efficient Overall Water Splitting

Feili Lai, Jianrui Feng, Xiaobin Ye, Wei Zong, Guanjie He, Yue-E Miao,* Xuemei Han, Xing Yi Ling, Ivan P. Parkin, Bicao Pan, Yongfu Sun,* Tianxi Liu*

F. L. Lai, J. R. Feng, W. Zong, Dr. Y. E. Miao, Prof. Dr. T. X. Liu
State Key Laboratory for Modification of Chemical Fibers and Polymer Materials
College of Materials Science and Engineering, Innovation Center for Textile Science
and Technology
Donghua University
Shanghai 201620, P. R. China
Email: txliu@dhu.edu.cn or yuee_miao@dhu.edu.cn

F. L. Lai, X. B. Ye, Prof. B. C. Pan, Prof. Dr. Y. F. Sun
Hefei National Laboratory for Physical Science at the Microscale
University of Science and Technology of China
Hefei, Anhui 230026, P. R. China
Email: yfsun@ustc.edu.cn

Dr. G.J. He, Prof. Dr. I.P. Parkin
Christopher Ingold Laboratory
Department of Chemistry
University College London
20 Gordon Street, London WC1H 0AJ, U.K.

Dr. X.M. Han, Prof. Dr. X. Y. Ling
Division of Chemistry and Biological Chemistry
School of Physical and Mathematical Sciences
Nanyang Technological University
21 Nanyang Link, Singapore 637371

Table of contents

1. Material synthesis

2. Supporting Figures and Tables

3. References

1. Materials synthesis and characterization:

Synthesis of ZIF-67. Chemical reagents of analytical grade were utilized directly without any purification. For the synthesis of ZIF-67, $\text{Co}(\text{NO}_3)_2 \cdot 6\text{H}_2\text{O}$ (249 mg, 1.0 mmol) and 2-methylimidazole (328 mg, 4.0 mmol) were dissolved in 25 mL of methanol to form two clear solutions. Then, the solution of 2-methylimidazole was subsequently poured into the solution of $\text{Co}(\text{NO}_3)_2 \cdot 6\text{H}_2\text{O}$. After the solutions were mixed and stirred at room temperature for 24 h, the purple precipitates were centrifuged and washed with methanol several times and dried at 60 °C.

Synthesis of hollow nitrogen-doped carbon polyhedron (HNCP). 20 μL of aniline monomer were subsequently added into 100 mL of ZIF-67 dispersion (1 mg mL^{-1}) under sonication. Then, 0.95 g of $(\text{NH}_4)_2\text{S}_2\text{O}_8$ dissolved in 30 mL of deionized water was added, and stirred overnight. The resulting precipitates were washed with deionized water and dried at 60 °C and are denoted as ZIF-67@PANI. For the removal of ZIF-67 template, ZIF-67@PANI was stirred in HCl solution (1 mol L^{-1}) for 6 h at room temperature, thus obtaining hollow PANI polyhedron. The hollow PANI polyhedron was placed in a tube furnace, heated to 800 °C with a ramp rate of 5 °C min^{-1} , and kept for 3 h in N_2 flow, to yield hollow nitrogen-doped carbon polyhedron (NHCP).

Synthesis of transition-metal doped NiCo_2O_4 @HNCP (TM- NiCo_2O_4 @HNCP). For the preparation of different TM- NiCo_2O_4 @HNCP samples, 110 mg of $\text{Ni}(\text{NO}_3)_2 \cdot 6\text{H}_2\text{O}$, 221 mg of $\text{Co}(\text{NO}_3)_2 \cdot 6\text{H}_2\text{O}$, and 560 mg of methenamine (HMT) were added into 30 mL of ethanol/water (v:v = 1:1) solution with 6×10^{-5} mol of the corresponding metal ion from FeCl_2 , $\text{Zn}(\text{NO}_3)_2 \cdot 6\text{H}_2\text{O}$, $\text{Cu}(\text{NO}_3)_2$, $\text{Mn}(\text{NO}_3)_2$, respectively. After sonication for 10 min, 20 mg of HNCP was dispersed into the above clear solution with another 2 h of sonication. The reaction solution was

transferred to a 50 mL flask, and then heated in an oil bath at 80 °C for 8 h. The product was collected by centrifugation, washed with deionized water/ethanol, and dried at 60 °C. Then, the powder was annealed in a tubular furnace at 350 °C for 2 h in a N₂ gas atmosphere with a ramp rate of 5 °C min⁻¹. For comparison, NiCo₂O₄@HNCP was synthesized using the same steps except for adding the metal salt.

Synthesis of Fe-ZnNi@HNCP. For the preparation of Fe-ZnNi@HNCP, 113 mg of Ni(NO₃)₂·6H₂O, 221 mg of Ni(NO₃)₂·6H₂O, 34 mg of NaNO₃, and 6 × 10⁻⁵ mol of FeCl₂ and 30% hydrogen peroxide solution were added into 30 mL solution. After sonicated for 10 min, 20 mg of HNCP was dispersed into the above clear solution. After mixing all the precursors, the above solution was stirred under a nitrogen atmosphere at room temperature, to adjust its pH to 8 by adding 1 M NaOH solution. After the completion of the reaction, the product was collected by centrifugation, washed with deionized water/ethanol, and dried at 60 °C. Then, the powder was annealed in a tubular furnace at 350 °C for 2 h under N₂ gas atmosphere with a ramp rate of 5 °C min⁻¹. For comparison, ZnNi@HNCP was synthesized using the same steps except for adding metal salt.

Synthesis of Fe-Co@HNCP. For the preparation of Fe-Co@HNCP, 331 mg of Co(NO₃)₂·6H₂O, 560 mg of HMT, and 9 × 10⁻⁵ mol of FeCl₂ were added into 30 mL of ethanol/water (1:1 v/v) solution. After sonicated for 10 min, 20 mg of HNCP was dispersed into the clear solution followed by another 2 h of sonication. The reaction solution was transferred into a 50 mL flask, and then heated in an oil bath at 80 °C for 8 h. The product was collected by centrifugation, washed with deionized water/ethanol, and dried at 60 °C. Then, the powder was annealed in a tubular furnace at 350 °C for 2 h under N₂ gas atmosphere with a ramp rate of 5 °C min⁻¹. For comparison, Co@HNCP was synthesized using the same steps except for adding the metal salt.

2. Supporting Figures and Tables:

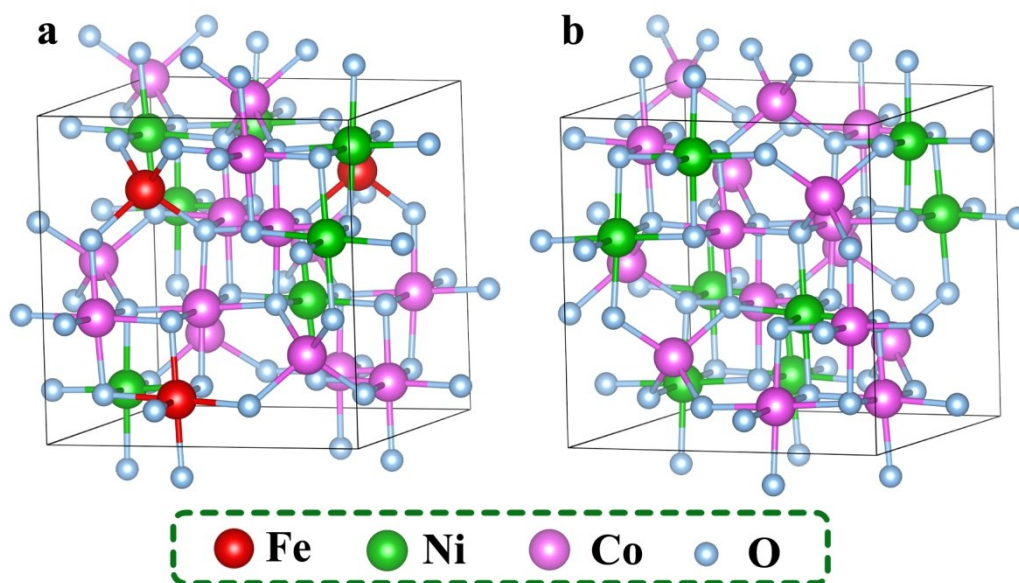


Figure S1. Optimized crystal structures for (a) Fe-NiCo₂O₄ and (b) pristine NiCo₂O₄.

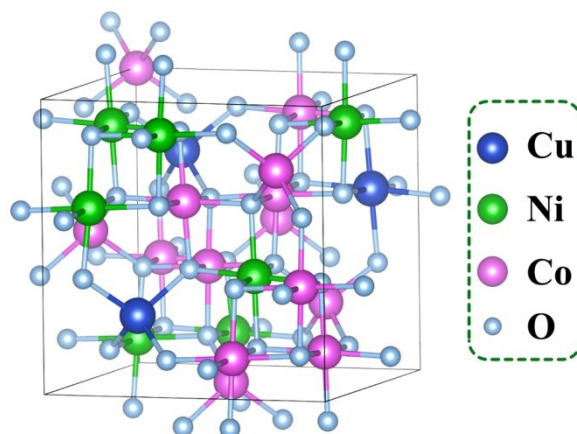


Figure S2. The optimized crystal structure for Cu-NiCo₂O₄.

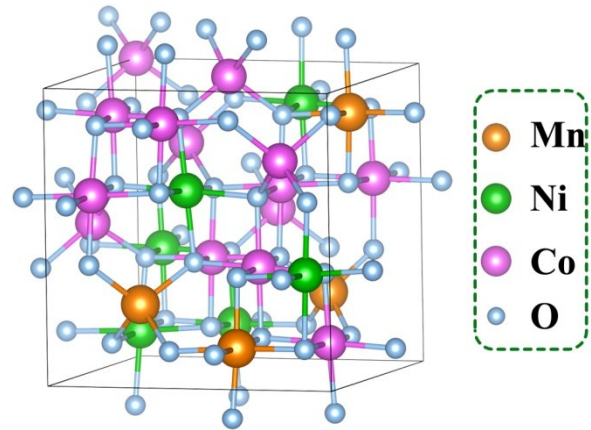


Figure S3. The optimized crystal structure for Mn-NiCo₂O₄.

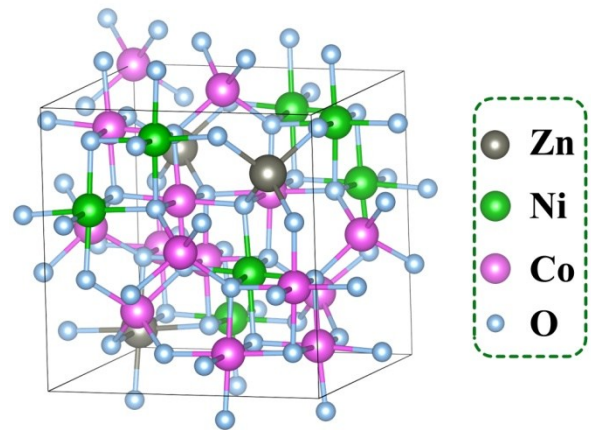


Figure S4. The optimized crystal structure for Zn-NiCo₂O₄.

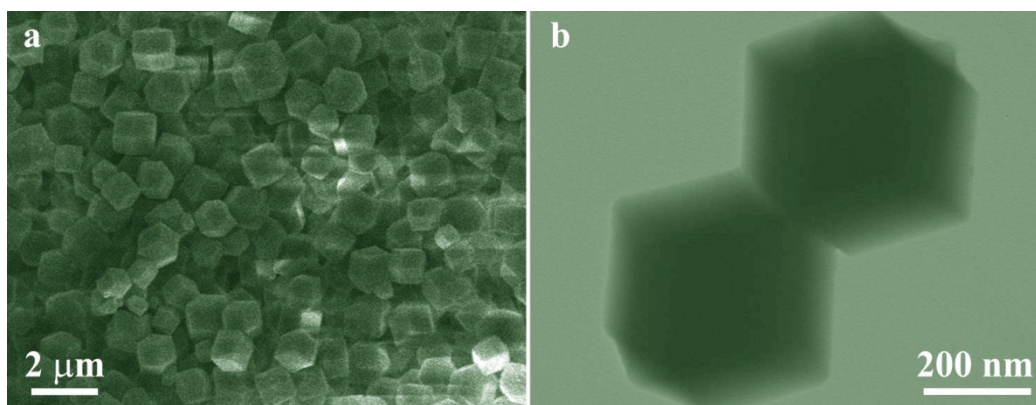


Figure S5. (a) Scanning electron microscopy (SEM) and (b) transmission electron microscopy (TEM) images of ZIF-67 crystals.

The ZIF-67 crystals of rhombic dodecahedral shape with a diameter of 500 nm (Figure S5) were obtained by mixing the methanolic solutions of cobalt nitrate and dimethylimidazole, and keeping the reaction at room temperature.

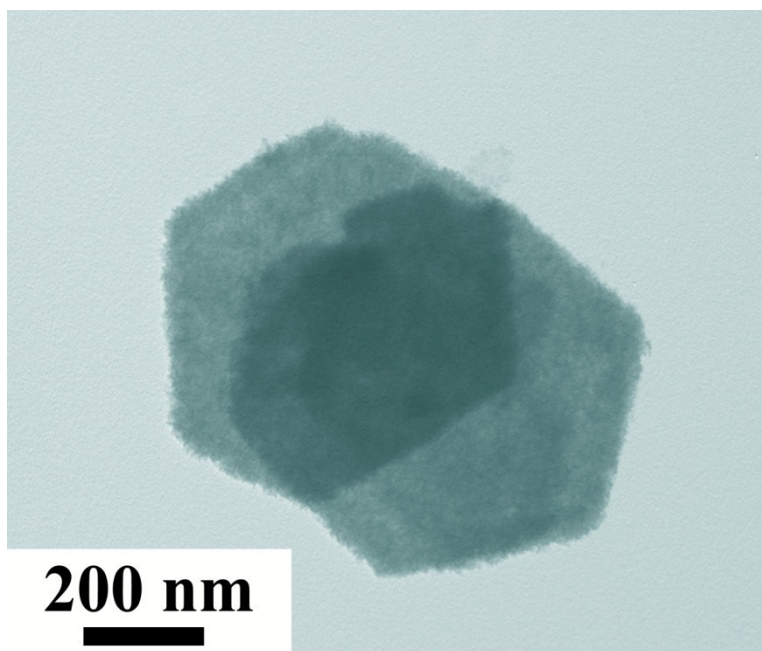


Figure S6. TEM image of ZIF-67@polyaniline.

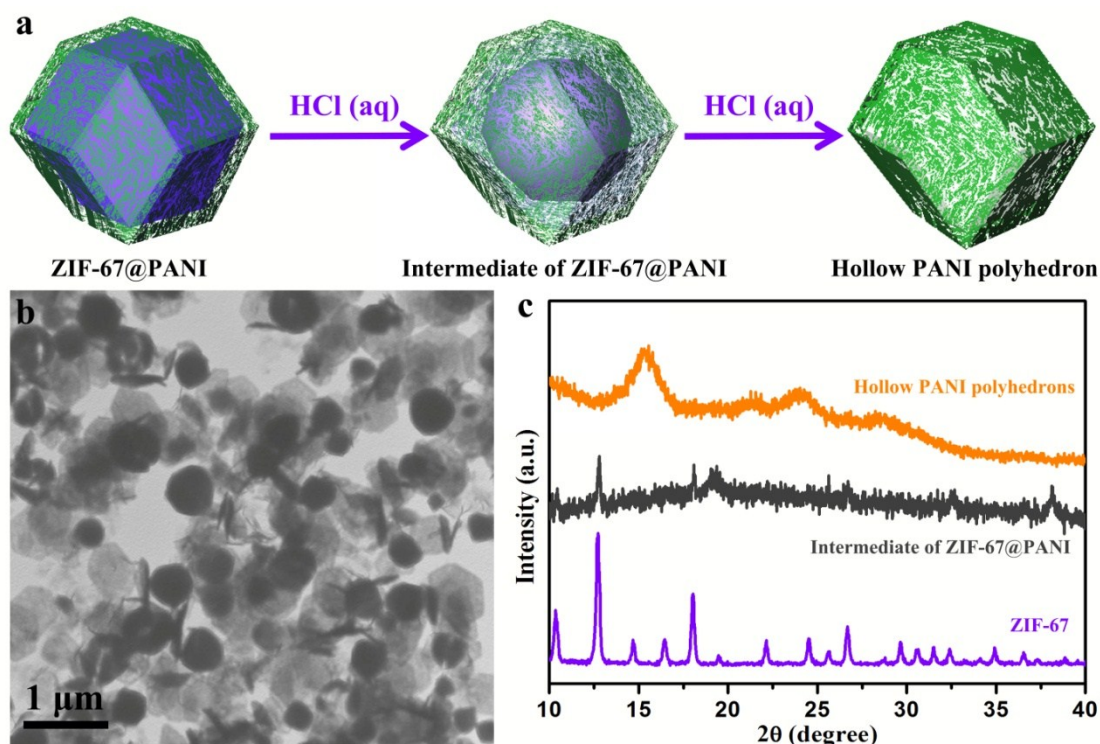


Figure S7. (a) Schematic illustration of the formation process of hollow PANI polyhedrons. (b) TEM image of the intermediate of ZIF-67@PANI. (c) XRD patterns of ZIF-67, intermediate of ZIF-67@PANI and hollow PANI polyhedrons.

The structural evolution process from solid ZIF-67@PANI to hollow PANI polyhedron is displayed in Figure S7a, during which the ZIF-67 core is etched gradually by dilute hydrochloric acid solution. As a result, the ZIF-67 template is removed, leading to the successful retention of the hollow PANI polyhedron. During the etching process of ZIF-67@PANI, an intermediate state can be observed with the residual ZIF-67 crystals (Figure S7b). Meanwhile, the XRD patterns also reveal a similar phenomenon. As shown in Figure S7c, the relative intensity and peak position of ZIF-67 in the XRD patterns are in agreement with previous reports.^(1,2) The final hollow PANI polyhedrons display four broad peaks centered at $2\theta = 15.4^\circ$, 21.2° , 24.7° and 28.7° , indicating its amorphous character. The weaker relative intensity of ZIF-67 proves the partial structural collapse in the intermediate of ZIF-67@PANI, as a transition stage for hollow PANI polyhedron formation.

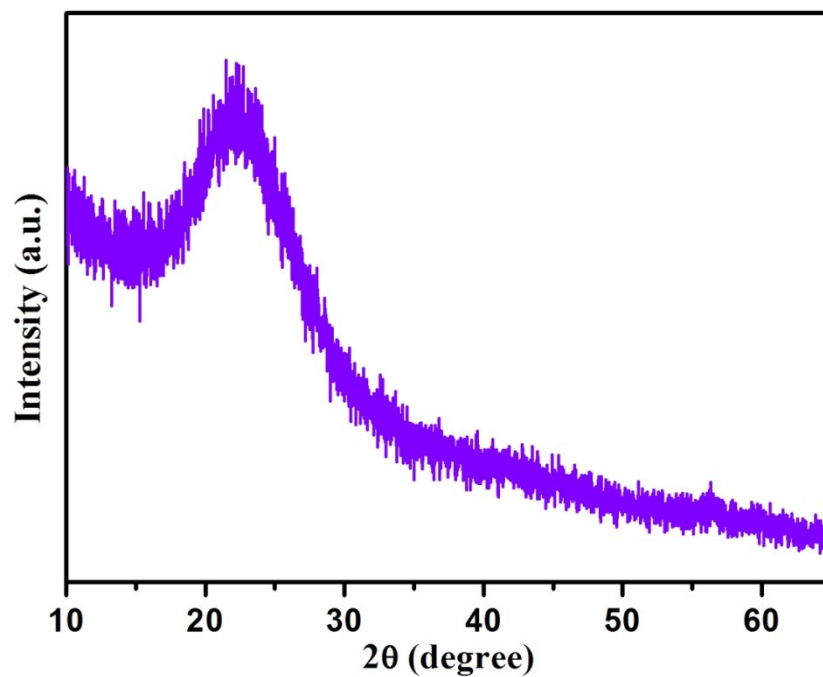


Figure S8. X-ray diffraction (XRD) pattern of HNCP.

The obvious peak at $2\theta = 22.4^\circ$ belongs to a typical (002) interlayer space of graphite-type carbon (Figure S8), indicating an amorphous structure of the nitrogen-doped carbon template of hollow NC polyhedrons.

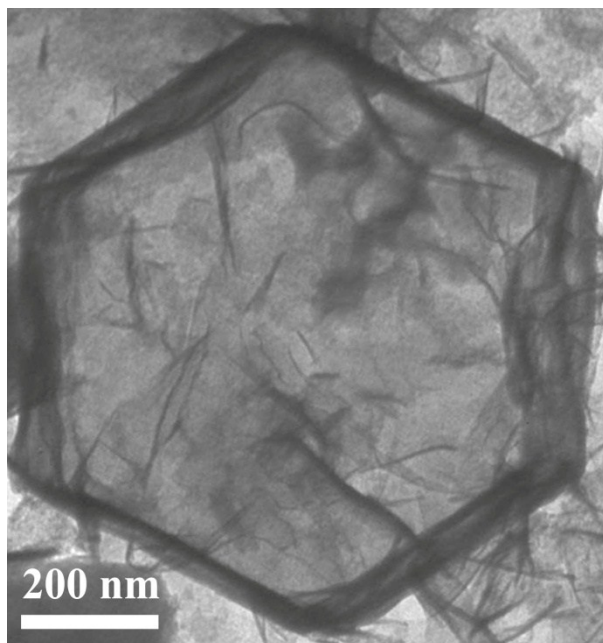


Figure S9. TEM image of Fe-NiCo LDH@HNCP.

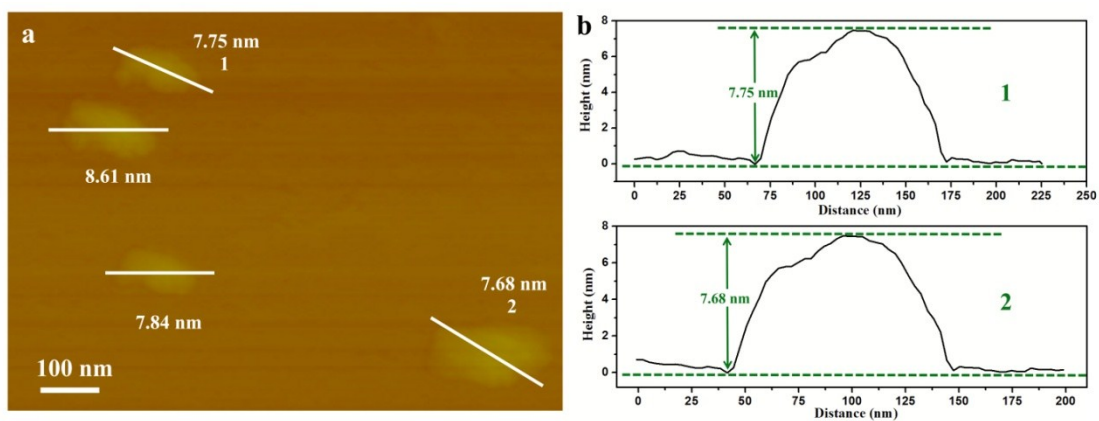


Figure S10. (a) AFM image, and (b) the corresponding height profile of Fe-doped NiCo_2O_4 nanosheets from the as-prepared $\text{Fe-NiCo}_2\text{O}_4\text{@HNCP}$.

As shown in Figure S10a and S10b, the height of $\text{Fe-NiCo}_2\text{O}_4$ nanosheets is approximately 8.0 nm, which is about decuple the value of 0.8 nm for the unit-cell dimensions given for NiCo_2O_4 (JCPDS 73-1702).

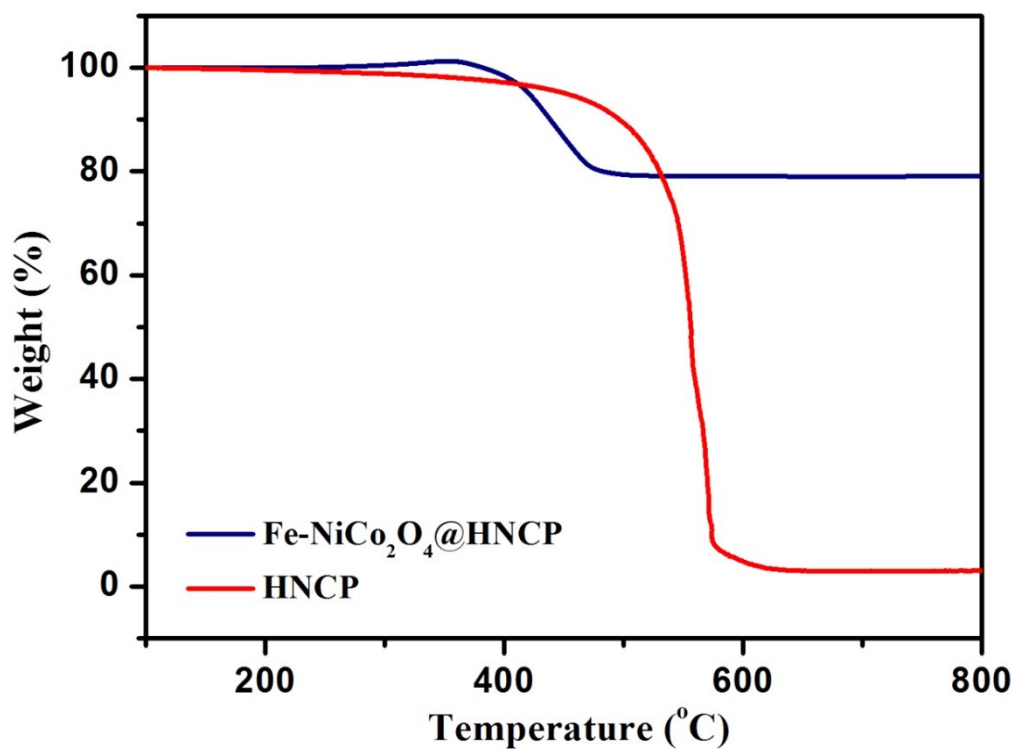


Figure S11. TGA profiles of Fe-NiCo₂O₄@HNCP and HNCP.

The weight ratio of Fe-NiCo₂O₄ nanosheet in the Fe-NiCo₂O₄@HNCP is determined by thermogravimetric analysis (TGA) to be around 80 wt% (Figure S11), which is close to the theoretical mass loading of Fe-NiCo₂O₄ nanosheets of 82 wt%, indicating the high loading percentage during the synthesis process.

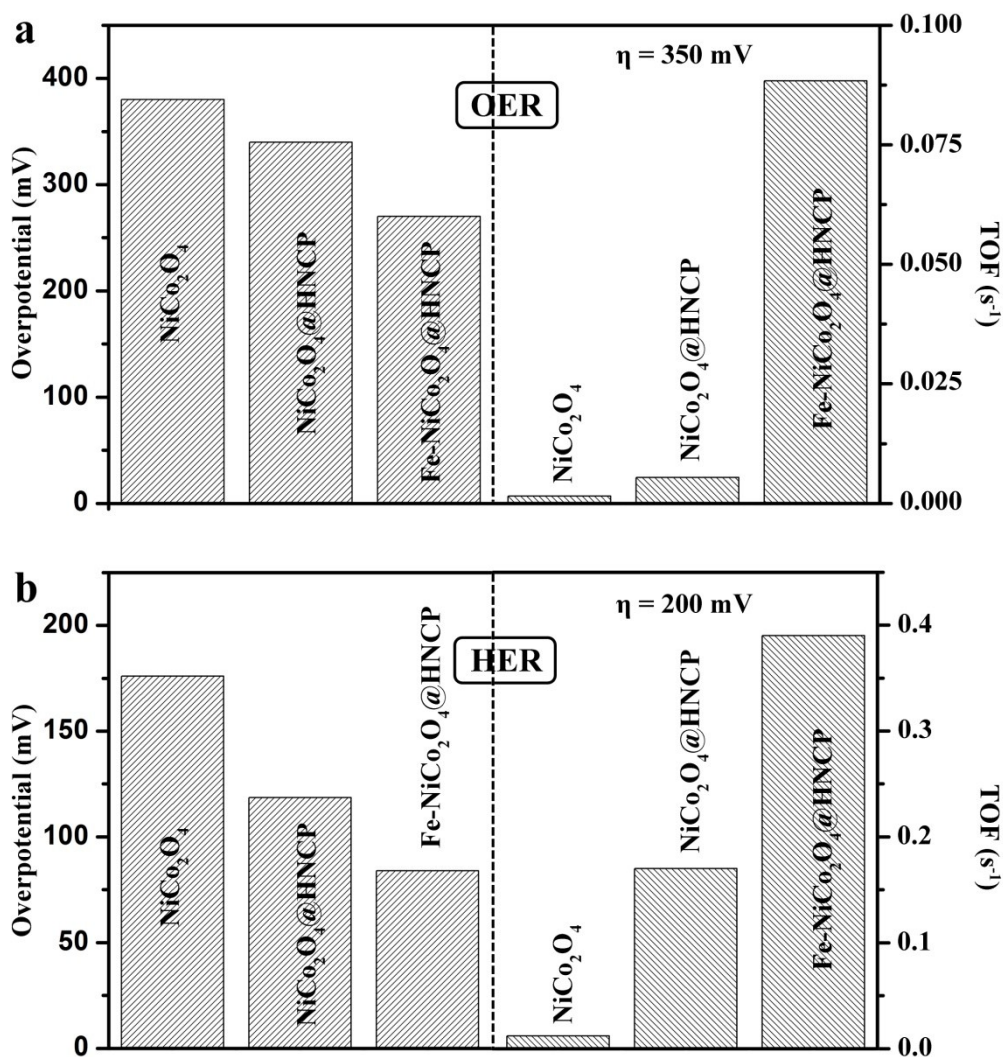


Figure S12. (a) Comparison of overpotentials (left panel) and the corresponding TOF values at $\eta = 350 \text{ mV}$ (right panel) of varied samples for OER. (b) Comparison of overpotentials (left panel) and the corresponding TOF values at $\eta = 200 \text{ mV}$ (right panel) of varied samples for HER.

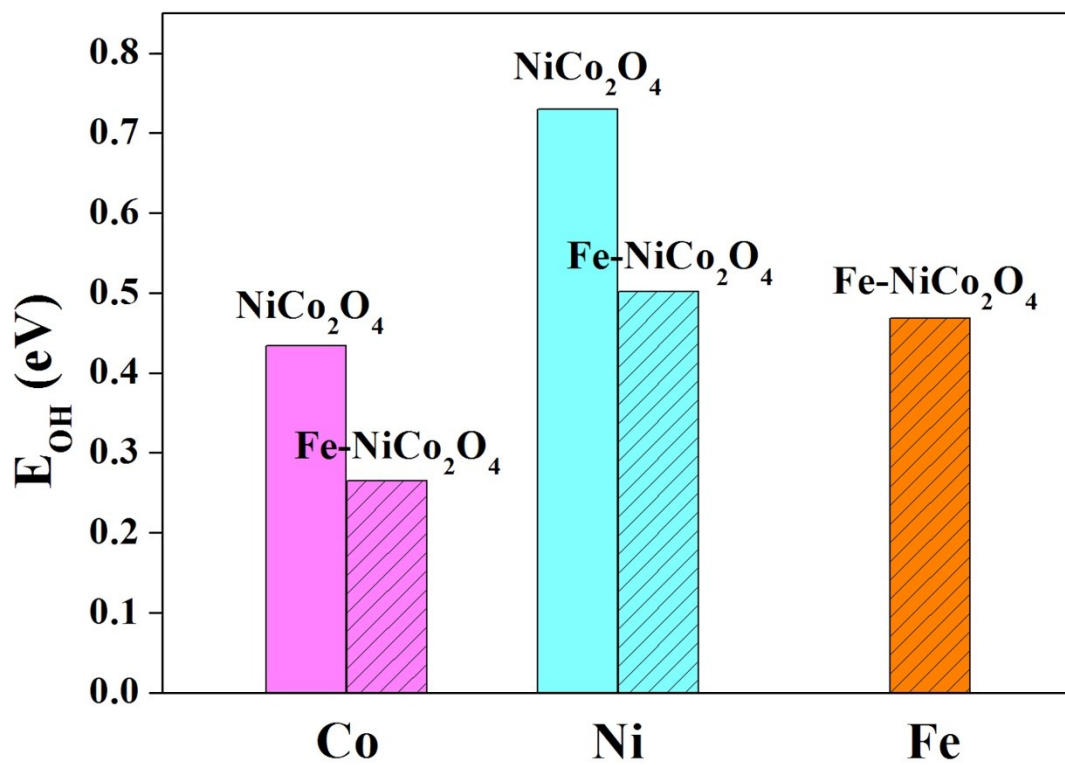


Figure S13. Calculated adsorption energy toward OH⁻ on different metal sites (Co, Ni, and Fe) of Fe-NiCo₂O₄.

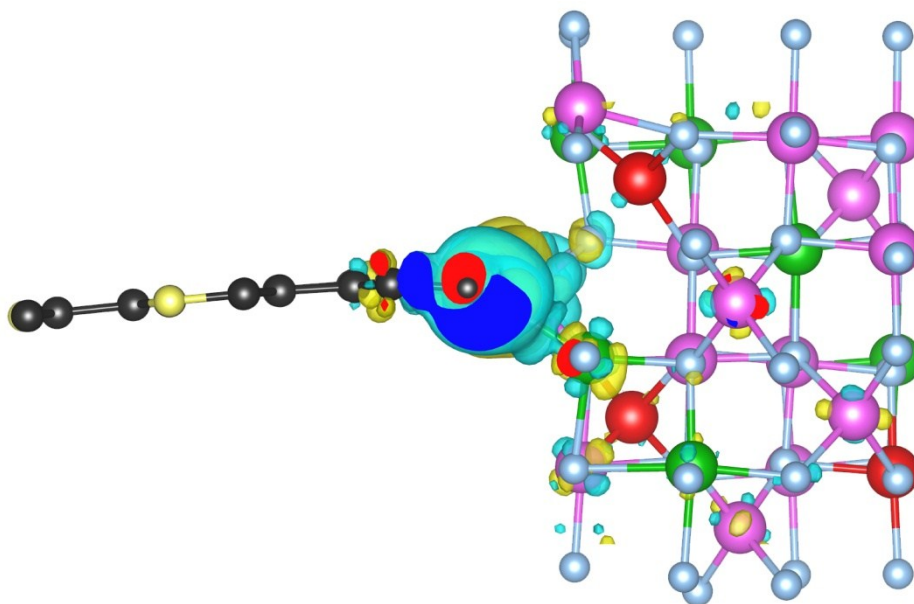


Figure S14. Charge density distribution around the interface between HNCP and Fe-NiCo₂O₄ for Fe-NiCo₂O₄@HNCP.

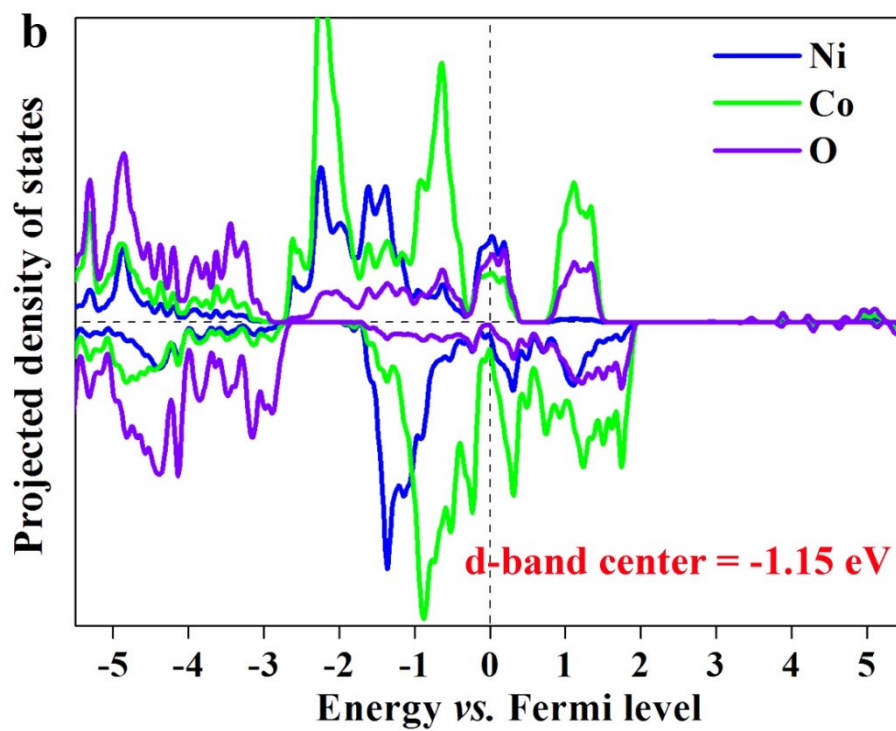
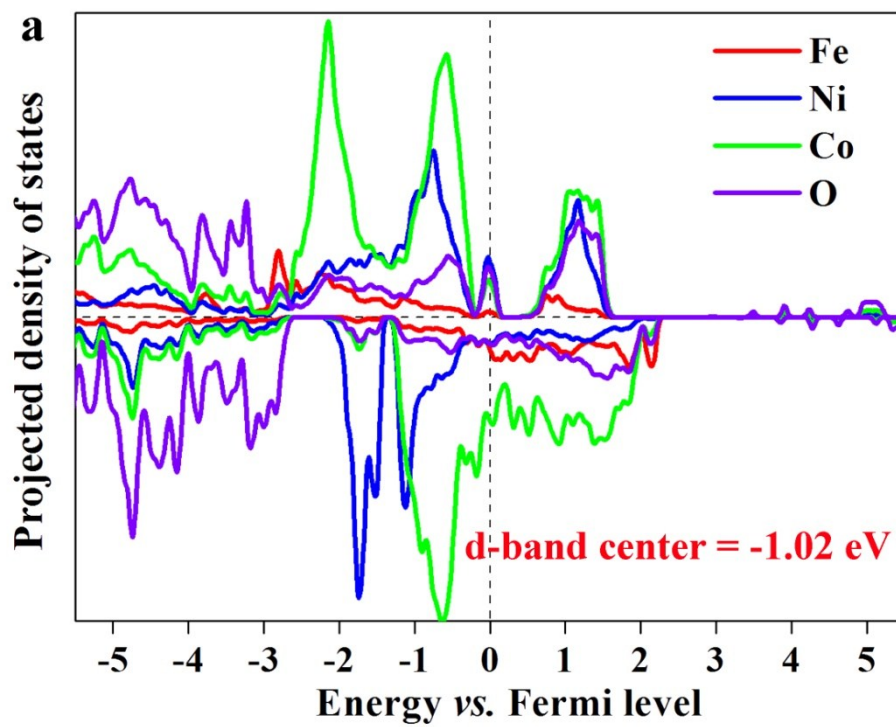


Figure S15. Calculated DOS for (a) Fe-NiCo₂O₄, and (b) NiCo₂O₄.

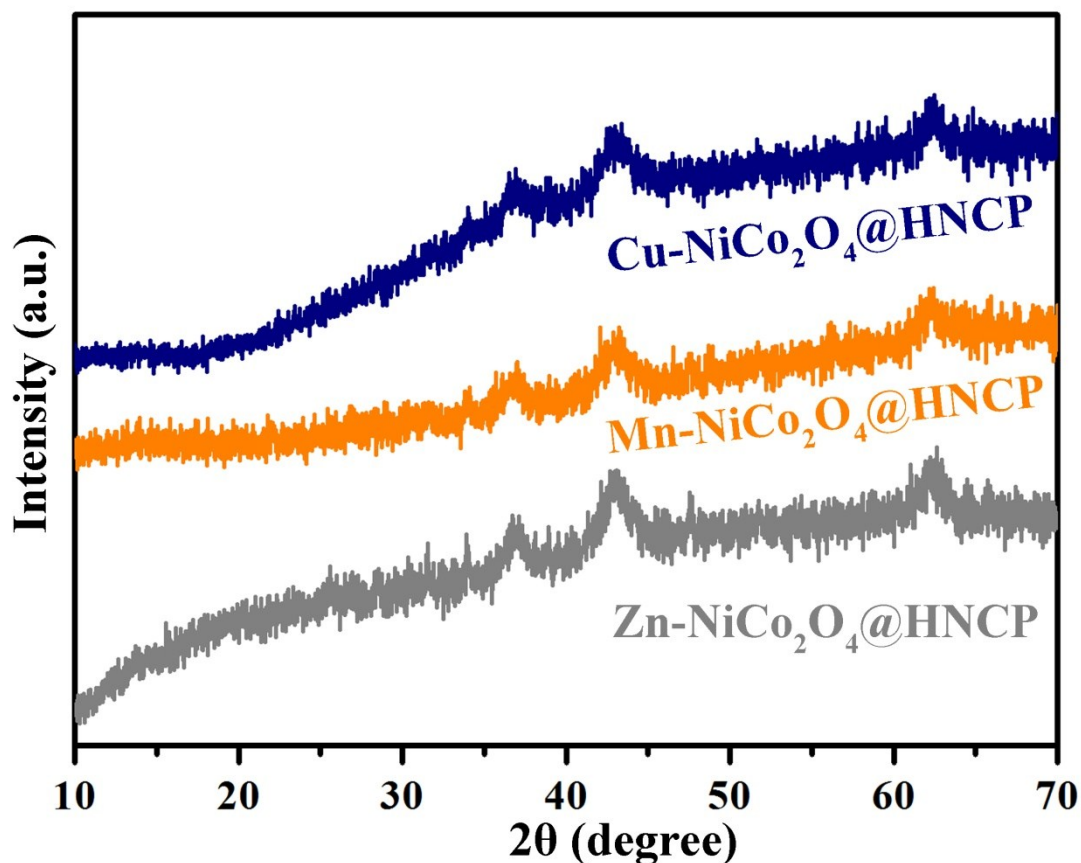


Figure S16. X-ray diffraction (XRD) patterns of Cu-NiCo₂O₄@HNCP, Mn-NiCo₂O₄@HNCP, and Zn-NiCo₂O₄@HNCP.

As shown in Figure S16, the X-ray diffraction (XRD) patterns show the almost identical crystal structure among various transition-metal doped NiCo₂O₄, including Cu-NiCo₂O₄@HNCP, Mn-NiCo₂O₄@HNCP, and Zn-NiCo₂O₄@HNCP. The peaks at $2\theta = 31.3^\circ, 37.2^\circ, 43.9^\circ, 58.3^\circ, \text{ and } 63.5^\circ$ can be well indexed to (220), (311), (400), (511), and (440) planes, respectively, indicating the good maintaining of spinel structures of Cu-NiCo₂O₄, Mn-NiCo₂O₄, and Zn-NiCo₂O₄.

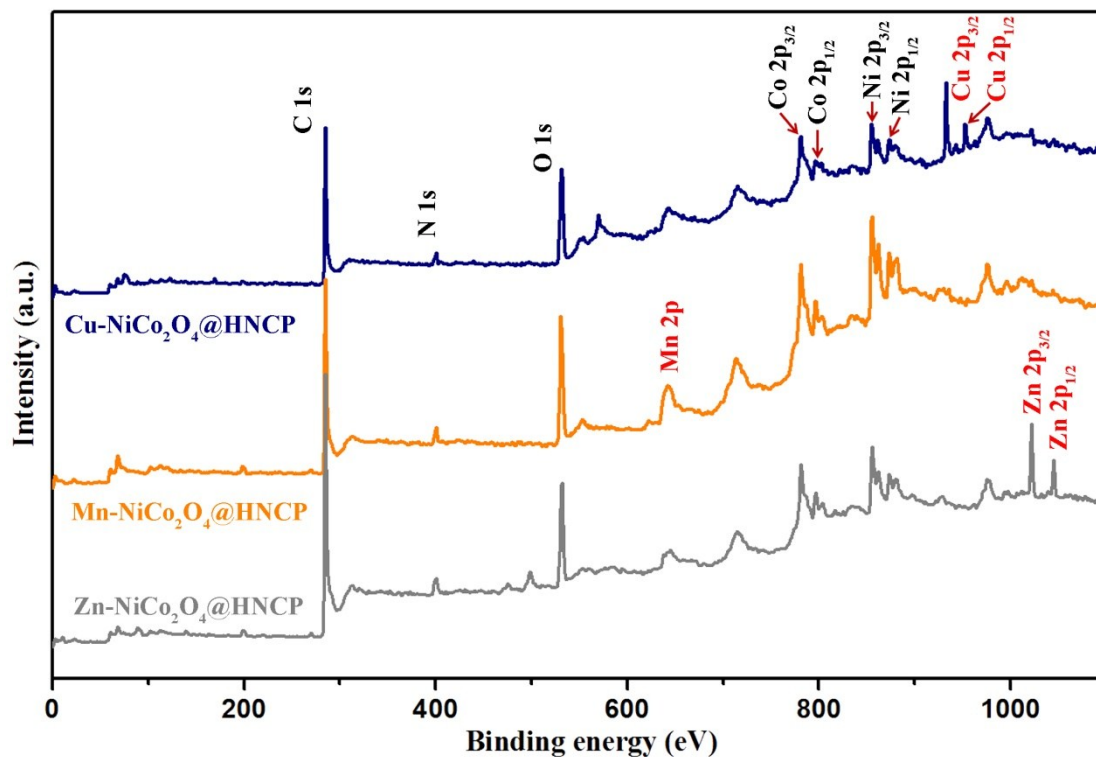


Figure S17. Survey scan spectra of Cu-NiCo₂O₄@HNCP, Mn-NiCo₂O₄@HNCP, and Zn-NiCo₂O₄@HNCP.

The full XPS spectra of Cu-NiCo₂O₄@HNCP, Mn-NiCo₂O₄@HNCP, and Zn-NiCo₂O₄@HNCP (Figure S17) contains the essential signals of C, O, N, Ni, and Co. The additional signal of Cu, Mn, Zn elements for the corresponding samples indicate the successful doping of these transition-metals in the structure of NiCo₂O₄.

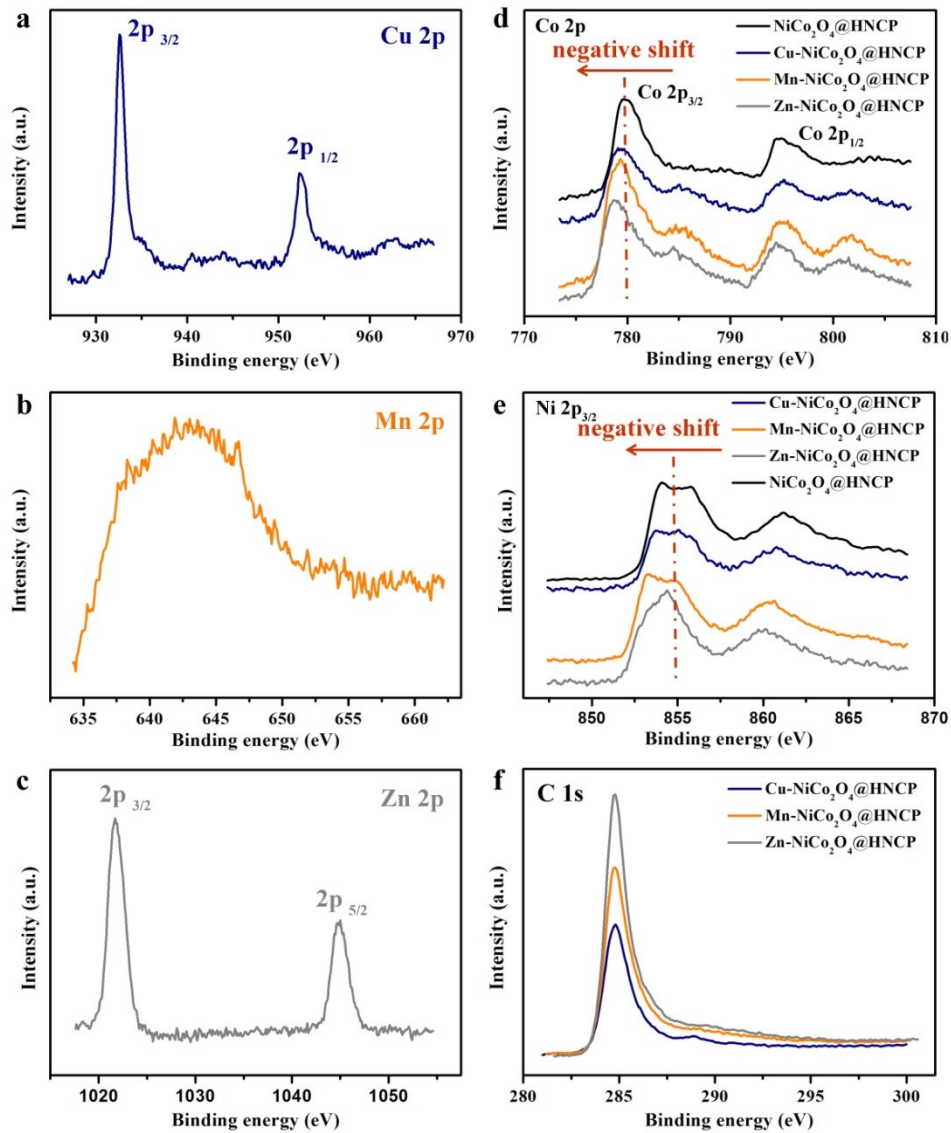


Figure S18. XPS spectra of (a) Cu 2p in $Cu-NiCo_2O_4@HNCP$, (b) Mn 2p in $Mn-NiCo_2O_4@HNCP$, and (c) Zn 2p in $Zn-NiCo_2O_4@HNCP$. (d) Co 2p, and (e) Ni 2p spectra in $Cu-NiCo_2O_4@HNCP$, $Mn-NiCo_2O_4@HNCP$, $Zn-NiCo_2O_4@HNCP$, and $NiCo_2O_4@HNCP$, respectively. (f) C 1s spectra in $Cu-NiCo_2O_4@HNCP$, $Mn-NiCo_2O_4@HNCP$, and $Zn-NiCo_2O_4@HNCP$, respectively.

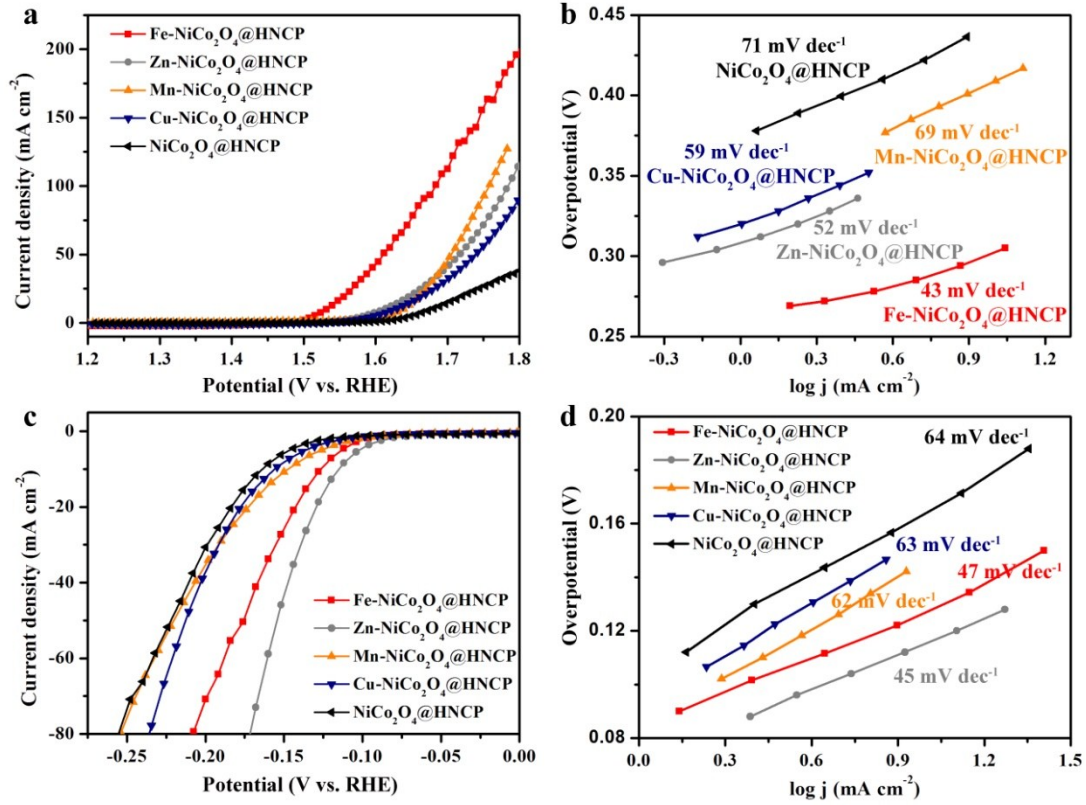


Figure S19. (a) Polarization curves, and (b) Tafel curves of TM-NiCo₂O₄@HNCP and NiCo₂O₄@HNCP samples in 1.0 M KOH solution for OER with a scan rate of 5 mV s⁻¹. (c) Polarization curves, and (d) Tafel curves of TM-NiCo₂O₄@HNCP and NiCo₂O₄@HNCP samples in 1.0 M KOH solution for HER with a scan rate of 5 mV s⁻¹.

As shown in Figure S19a and S19c, transition-metal doping significantly increases the electrocatalytic activities of TM-NiCo₂O₄@HNCP toward water splitting, among which Fe- and Zn-doped catalysts exhibit better electrocatalytic activities. The overpotentials of Zn-NiCo₂O₄@HNCP are 384 and 116 mV at current density of 10 mA cm⁻², for OER and HER respectively. The higher activity of Fe- and Zn-doping may be attributed to their enhanced effect for charge delocalization, with more active sites for electrolyte adsorption and accelerated electron mobility. The above-analyzed results indicate that the electrocatalytic activity of NiCo₂O₄ component can be optimized through different transition-metal doping, which is also proved by their Tafel plots (Figure S19b and S19d).

Table S1. Elemental contents (Fe, Co, and Ni) in Fe-NiCo₂O₄@HNCP by using EDX spectroscopy analyse.

Chemical elements	Weight percent (%)
Fe	2.9
Ni	19.3
Co	38.5

Table S2. Summary of various Ni-Co-based catalysts for OER in 1 M KOH.

Catalysts	Overpotential @ j_{10} (mv)	Tafel slope (mV dec ⁻¹)	References
Fe-NiCo₂O₄@HNCP	300	42	This work
Zn-NiCo₂O₄@HNCP	384	52	This work
Mn-NiCo₂O₄@HNCP	409	69	This work
Cu-NiCo₂O₄@HNCP	400	59	This work
NiCo₂O₄@HNCP	451	71	This work
Co₃O₄/NiCo₂O₄ DSNCs	340	88	<i>J. Am. Chem. Soc.</i> 2015 , 137, 5590
NiCo₂N/Ni foam	290	65	<i>ChemSusChem</i> 2017 , 10, 4170
CoN/Ni foam	300	69	<i>ChemSusChem</i> 2017 , 10, 4170
Hierarchical Ni-Co oxides	340	51	<i>Adv. Energy Mater.</i> 2015 , 5, 1500091
NiCoP microspheres	340	86	<i>Adv. Mater. Interfaces</i> 2016 , 3, 1500454
CoFeNiO_x/NF	240	-	<i>J. Am. Chem. Soc.</i> 2016 , 138, 8946
Ni_xCo_{3-x}O₄	370	59-64	<i>Adv. Mater.</i> 2010 , 22, 1926
rGO@CoNiO_x	320	45	<i>Adv. Funct. Mater.</i> 2017 , 27, 1606325
NiCoP/C nanoboxes	330	96	<i>Angew. Chem.</i> 2017 , 129, 3955
NiCo-mixed-oxide nanocage	380	50	<i>Adv. Mater.</i> 2016 , 28, 4601
NiCo₂O₄ microcuboids	290	53	<i>Angew. Chem. Int. Ed.</i> 2016 , 55, 6290
NiCo₂O₄ nanowire film	320	63	<i>Nano Energy</i> 2015 , 11, 333
Ni_{0.33}Co_{0.67}S₂ NWs	370	60	<i>Adv. Energy Mater.</i> 2015 , 5, 1402031
NiCo₂O₄ nanowire arrays	-	62	<i>Electrochim. Acta</i> 2015 , 174, 1216
Au/NiCo₂O₄ NR array	360	63	<i>ChemCatChem</i> 2014 , 6, 2501
PNG-NiCo	-	156	<i>ACS Nano</i> 2013 , 7, 10190
NiCo₂O₄ nanowire array	540	90	<i>J. Mater. Chem. A</i> 2014 , 2, 20823
Co-Ni₃N	307	57	<i>Adv. Mater.</i> 2018 , 1705516

Table S3. Summary of various Ni-Co-based catalysts for HER in 1 M KOH.

Catalysts	Overpotential @ j_{10} (mV)	Tafel slope (mV dec ⁻¹)	References
Fe-NiCo₂O₄@HNCP	124	47	This work
Zn-NiCo₂O₄@HNCP	116	45	This work
Mn-NiCo₂O₄@HNCP	146	62	This work
Cu-NiCo₂O₄@HNCP	157	63	This work
NiCo₂O₄@HNCP	164	64	This work
NiCo ₂ N/Ni foam	290	79	<i>ChemSusChem</i> 2017 , 10, 4170
NiCo ₂ O ₄ microcuboids	110	49	<i>Angew. Chem. Int. Ed.</i> 2016 , 55, 6290
Co-Ni ₃ N	194	156	<i>Adv. Mater.</i> 2018 , 1705516
Ni _{0.69} Co _{0.31} P	167	47	<i>Nanoscale</i> 2016 , 8, 19129
Ni-Co-P-300	150	61	<i>Chem. Commun.</i> 2016 , 52, 1633
NiCoP/rGO	209	124	<i>Adv. Funct. Mater.</i> 2016 , 26, 6785
Co ₄ Ni ₁ P NTs	129	52	<i>Adv. Funct. Mater.</i> 2017 , 27, 1703455
NiCo ₂ S ₄ /CC	200-305	141	<i>Nanoscale</i> 2015 , 7, 15122
Ni-Co sulphide	-	81	<i>Int. J. Hydrog. Energy</i> 1991 , 16, 1
Ni _{0.33} Co _{0.67} S ₂ NWs	88	118	<i>Adv. Energy Mater.</i> 2015 , 5, 1402031

3. References:

- (1) Yang, J.; Zhang, F. J.; Lu, H. Y.; Hong, X.; Jiang, H. L.; Wu, Y. E.; Li, Y. D. Hollow Zn/Co ZIF Particles Derived from Core-Shell ZIF-67@ZIF-8 as Selective Catalyst for the Semi-Hydrogenation of Acetylen. *Angew. Chem. Int. Ed.* **2015**, *54*, 10889-10893.
- (2) Kwon, H. T.; Jeong, H.; Lee, A. S.; An, H. S.; Lee, J. S. Heteroepitaxially Grown Zeolitic Imidazolate Framework Membranes with Unprecedented Propylene/Propane Separation Performances. *J. Am. Chem. Soc.* **2015**, *137*, 12304-12311.